Impact of preferential flow on soil chemistry of a podzol

Christina Bogner[a,*], Werner Borken[b], Bernd Huwe[c]

[a]*Ecological Modelling, BayCEER, University of Bayreuth, Dr.-Hans-Frisch-Straße 1-3, 95448 Bayreuth, Germany*
[b]*Soil Ecology, BayCEER, University of Bayreuth, Dr.-Hans-Frisch-Straße 1-3, 95448 Bayreuth, Germany*
[c]*Soil Physics Group, BayCEER, University of Bayreuth, 95440 Bayreuth, Germany*

Abstract

Preferential flow paths are thought to affect the patterns of chemical properties of forest soils. However, little is known about their influence on podzols in coniferous forests. In our study we examined how soil chemical properties of a podzol in a Norway spruce stand are affected by preferential flow. We did three tracer experiments with Brilliant Blue FCF and analyzed soil chemical parameters (exchangeable cations, pH, total C, total N and C:N ratio) of preferential flow paths and soil matrix. For statistical analysis, we used mixed-effects models to account for a hierarchical sampling of our data. We found 5.0 g kg^{-1} more C, 0.24 g kg^{-1} more N, a C:N ratio larger by 2, smaller pH values (0.16 pH units), 32% more Ca and 57% more Mg in preferential flow paths than in soil matrix. Compared to the adjacent soil matrix, the content of Al did not differ significantly. However, 67% more Fe were found in preferential flow paths. These distinct chemical properties are probably due to root exudates, transport of solutes and dissolved organic carbon and percolation of acid soil solution from organic horizons along preferential paths. We attribute the increase of Ca and Mg to their transport via preferential flow paths after the application of lime some years ago. We conclude that a lower pH might enhance the release of Fe (and possibly Al) and thus increase podzolisation. In addition, our results show that soil liming affect both the topsoil and the subsoil via transport of basic cations along preferential flow paths.

Keywords: dye tracers, vadose zone, podzols, forest soils, preferential flow, patterns

1. Introduction

Podzols are soils that develop on sandy to loamy textured materials and occur in boreal, temperate and tropic regions (McKeague et al., 1983; Driessen et al., 2001). In temperate climates podzols are found at high altitudes, in mid-mountain ranges under coniferous vegetation or in heathlands ((Sauer et al., 2007) and the references therein). Typically, four main horizons can be distinguished: "[...] *a dark-colored organic surface horizon; a bleached eluvial horizon; a reddish, brownish or black illuvial horizon enriched in amorphous materials; and a sandy C horizon*" (McKeague et al., 1983).

---

*Corresponding author: Tel.: +49 921 555655; Fax: +49 921 555799
Email address: christina.bogner@uni-bayreuth.de (Christina Bogner)

In a review article Lundström et al. (2000) summarized the basic ideas of podzolisation: *mobilization - downward transport - immobilization* of Al and Fe. They outlined that Al and Fe can be removed from the eluvation horizon E by (a) complexation by organic acids and downward transport as soluble organo-metal-complexes or by (b) silicate weathering and downward transport as inorganic colloids, wherease mechanism (a) dominates in most soils. If Al and Fe are transported downwards as organo-metal-complexes, their immobilization in the illuvial B horizon is explained either by (a) precipitation/adsorption due to an increased C to metal ratio or by (b) microbial degradation of the organic ligand (Lundström et al., 2000). Buurman and Jongmans (2005) identified discrepancies between the existing podsolisation theories and field observation concerning the nature of organic matter and proposed a modification. Indeed, the above mentioned mechanisms suggest an immobilization of organic matter (OM) together with Al and Fe. However, according to Buurman and Jongmans (2005), in well-drained podzols with an intensely rooted B horizon, the accumulation of OM is mainly due to root debris and not to illuvation.

In our study we focus on the relationship between the podzolisation process and preferential flow of water in a podzol forest soil under Norway spruce. Preferential flow describes all phenomena where water flows through localized pathways bypassing a portion of the soil matrix (Hendrickx and Flury, 2001). Main transport mechanisms of preferential flow are inhomogeneous matrix flow and macropore flow. Hendrickx and Flury (2001) explained in their work that inhomogeneous matrix flow usually occurred in coarse-textured soils induced by textural differences or water repellency, for example. According to these authors, macropore flow was typical for highly structured soils or soils containing biopores like root channels or earthworm burrows.

Several studies showed that predominant flow paths could be stable for decades. Ritsema and Dekker (2000), for instance, observed that preferential flow paths reoccurred at the same locations during successive rain events in a water repellent sandy soil. They concluded that in soils without anthropogenic disturbance (e.g. untilled agricultural or forest soils) preferential flow paths might remain stable for an unlimited period of time. These findings accord well with results by Hagedorn and Bundt (2002). They estimated an age of about 40 years for preferential flow paths in a forest soil by measuring the distribution of radionuclides.

Due to temporal stability and reoccurrence of preferential flow at the same location, biological and chemical conditions in preferential flow paths and soil matrix are likely to differ. Bundt et al. (2001b), for example, found higher cation exchange capacity, base saturation, organic C and organic N concentrations in preferential flow paths of a forest soil. In addition, there were indications that soil organic matter in preferential flow paths was younger and N cycling faster than in the soil matrix (Bundt et al., 2001a). This is in accordance with Hagedorn et al. (1999) who reported an increased N transformation in preferential flow paths compared with the soil matrix. These authors mentioned that along flow paths nitrate concentrations were higher, denitrification activity after rainfalls increased and net nitrification started earlier after drying and was enhanced.

Previous studies on differences between preferential flow and soil matrix focused on microbial biomass (Vinther et al., 1999), included treatments like wood ash application (Bundt et al., 2001b) or considered agricultural soil (Wuest, 2009). In contrast, the aim of this work is to determine how soil chemical properties (concentration of exchangeable cations, pH, total C, total N and C:N ratio) are affected by preferential flow in a podzol under natural

conditions. Podzols have been studied for many years and a vast amount of literature on their occurrence and development exist. However, to our knowledge, the abundant studies on the chemistry of podzols do not distinguish between regions of preferential flow and the soil matrix.

The present work is part of a larger study on flow processes in a forest soil. In an earlier paper Bogner et al. (2010) analyzed the main flow mechanisms at the same study site by mixed-effects modeling. We identify preferential flow paths by dye tracer application and define them as dye stained areas. We hypothesize that preferential flow paths are locations of enhanced podzolisation compared to the adjacent soil matrix.

Most studies that investigated differences between preferential flow paths and soil matrix used the paired t-test or its non-parametric equivalent and analyzed different depths separately (e.g. Bundt et al., 2001b; Vinther et al., 1999). In contrast, we propose to employ mixed-effects models to account for the hierarchical nature of sampled data and spatial heterogeneities. This method allows us to consider all plots and all depths in one single analysis and model the covariance structure of the sampled data explicitly.

2. Materials and methods

2.1. Site description

The study site Coulissenhieb II is situated in the Lehstenbach catchment in southeast Germany (50°08′N, 11°52′E, 770 m above see level). This catchment is part of the Fichtelgebirge – a mountain ridge dominated by the Norway spruce (*Picea abies L.*) with wavy hair-grass (*Deschampsia flexuosa L.*) as main understorey vegetation (Gerstberger et al., 2004). The mean annual precipitation is about 1160 mm, with a maximum in December and a second maximum in July; and the mean annual air temperature equals approximately 5° C (Foken, 2003). This region has a continental temperate climate with a maritime character because of high precipitation (Gerstberger et al., 2004).

At Coulissenhieb II the soil is classified as Haplic Podzol (IUSS Working Group WRB, 2007) with five mineral soil horizons (AE, Bsh, Bs, Bw and Bw/C) with a sandy to loamy texture and a up to 15-cm thick mor-type organic layer consisting of Oi, Oe and Oa. Figure 1 summarizes the distribution of the soil fine fraction. The AE and the Bsh horizons are often discontinuous and have irregularly shaped boundaries (Bogner et al., 2010).

Schulze et al. (2009) reported extremely acidic pH_{CaCl_2} values ranging from 3.3 in Oa to 4.2 in the subsoil. They measured an organic C and total N contents in the Oa horizon of about 21% and 1% respectively that decreased with depth to 1% C and 0.2% N in Bw. Furthermore, according to Hentschel et al. (2007) the base saturation decreases with depth from 52% in Oa to 16% in Bw/C. They attributed this large value in the topsoil to an accidental diffuse application of dolomite ($CaMgCO_3$) between 1994 and 1999 by loss from a flying helicopter supposed to lime adjacent forest stands.

Stones play an important role at Coulissenhieb II site. Their content varies strongly within the site and with soil depth and ranges between few percent in the topsoil and up to 75% in the subsoil (Gerstberger et al., 2004). During our study at Coulissenhieb II we worked on three different experimental plots situated approximately 50 m apart that differed strongly in the content of large stones. While on plots 1 and 2 their content did not exceed
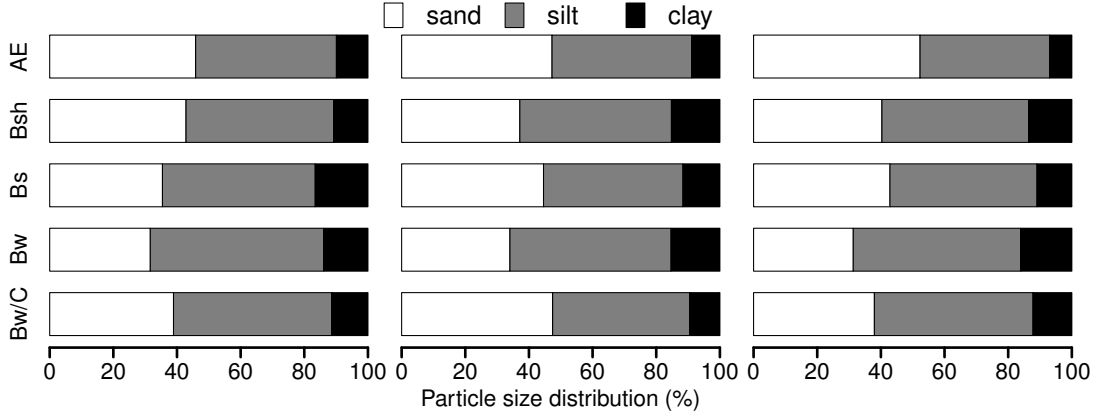
Figure 1: Distribution of the soil fine fraction (median of 1 to 7 samples per horizon and plot). Sand fraction corresponds to 2000–63 μm, silt to 63–2 μm and clay to <2 μm. Plots 1 to 3 are shown from left to right.

5%, a continuous layer of stones was present in the Bw (10–50%) and partly in the EA and Bsh horizons on plot 3.

2.2. Field and laboratory work

We did three tracer experiments with Brilliant Blue FCF (a sodium salt) and potassium iodide. Brilliant Blue is an organic dye that is often used for tracer studies in vadose zone hydrology (Flury et al., 1994; Forrer et al., 2000). It is well seen against most soil colors and according to Flury and Flühler (1994) its use in field studies is toxicologically acceptable. However, due to a non-linear interaction with the soil matrix, the dye might be retarded so that its patterns are different from those of infiltrating water (Ketelsen and Meyer-Windel, 1999; Kasteel et al., 2002). To assure that Brilliant Blue stained patterns were similar to infiltration patterns of water we used iodide as a reference tracer. Iodide patterns were visualized on two profiles per plot by sprinkling an iron(III) nitrate and starch solution on the soil (Lu and Wu, 2003).

The tracer solution was applied on a surface of about 2 m² with a rate of 64 mm h⁻¹ using an automated sprinkler (e.g. Ghodrati et al., 1990). The concentration of the tracers was 5 g l⁻¹ respectively. We did not remove the litter; however, we took away spruce cones to ensure a more homogenous application of the tracer solution. The day after irrigation, we prepared and photographed 11 vertical soil profiles of 1 m × 1 m. Bogner et al. (2010) described the analysis of these images. In this study, we used the dye coverage (amount of stained pixels on the photographs) to infer the importance of preferential flow. To this end, we calculated a mean dye coverage of the 11 stained profiles per plot.

Three profiles per plot were sampled for analysis of exchangeable cations (H, K, Na, Ca, Mg, Mn, Al, and Fe), content of total C and N, pH_{H_2O} and soil texture. We took bulk samples from Brilliant Blue stained and non-stained parts per soil horizon. To prevent any mixture of stained and non-stained material the soil was carefully scraped off the profile in fine layers. Some thin horizons were hardly stained and could not be sampled. Additionally, we could not sample the Bw/C horizon on plot 3 because only small amounts of the tracer penetrated below a stone layer situated in the Bw. Therefore, the number of samples differed from plot to plot resulting in 58 samples altogether. For further analysis, we grouped samples from Bw

and Bw/C and assigned them to Bw/C. Additional sampling and analysis comprised fine root density and soil bulk density. These results were described by Bogner et al. (2010).

Exchangeable cations were extracted with a 1M NH_4Cl solution and analyzed by ICP-OES (Inductively Coupled Plasma Optical Emission Spectrometry) (JY2000, Horiba, Ltd., Kyoto, Japan). Total C and N in soil samples were determined using a CNS-Analyser (Vario EL, Elementar Analysensysteme GmbH, Hanau, Germany). Total C should be equivalent to organic C because of acidic pH values. Indeed, we measured pH_{H_2O} values between 5.0 and 3.3. Furthermore, Hentschel et al. (2007) could not detect any carbonate in 9 soil pits at the same study site.

Brilliant Blue FCF ($C_{37}H_{34}N_2Na_2O_9S_3$, molar mass 792.9 g mol^{-1}) is an organic molecule consisting of 56% C and 4% N and its sorption on soil particles affects C and N contents of the soil. Therefore, the additional amount of C and N due to tracer application should be subtracted before further analysis. To this end, we determined the content of Brilliant Blue in soil by visible diffuse reflectance spectroscopy (Bogner et al., 2011). The predicted concentrations ranged from -0.5 g kg^{-1} soil to 3.9 g kg^{-1} soil. After transformation to C and N contents the positive predicted values were subtracted from the total C content and total N content, respectively. Samples with negative predicted values were not corrected. The maximum predicted value for additional C and N due to Brilliant Blue was 2.2 g kg^{-1} soil and 0.17 g kg^{-1} soil, respectively.

2.3. Initial data analysis

The tracer solution contained K and Na. Therefore, the content of these compounds in the soil was affected by the experiment. Consequently, their concentrations do not reflect the natural background in the soil and were excluded from further analysis. To find other possible disturbances due to tracer application, we performed a principal component analysis (PCA) on the log-transformed data set of exchangeable cations and pH. The latter was transformed to concentration of hydronium per g soil. The log-transformation was useful to reduce the influence of extreme points, for instance samples with especially high Ca content or very low pH. In two samples Mg concentrations were below the detection limit of the ICP-OES and we set them to $0.5 \times$ detection limit to avoid zeros. Additionally, we adjusted the Fe concentration of eight other samples the same way. As discussed above, we corrected the total C and N for the content of Brilliant Blue. Hence, C and N were not included in the PCA.

2.4. Mixed-effects models

In the present study we have to deal with missing values because the tracer bypassed some horizons. Another issue is the hierarchical sampling of the soil. Indeed, our data was not sampled randomly, but is grouped at three levels: plot, profile and horizon. Hierarchical sampling might induce dependencies in data and different sampling groups might have different variances (heteroscedasticity). In this case classical statistical techniques like ANOVA or ANCOVA are not applicable because they assume (a) homogeneity of variance, (b) independence of observations, (c) normally distributed residuals and do not allow for missing values. Consequently, we used mixed-effects models that contain fixed effects representing parameters of the entire population or certain repeatable levels of experimental factors (like horizons) and random effects associated with individual experimental units drawn at random

from a population (e.g. plot and profiles). Pinheiro and Bates (2000) pointed out in their work that this kind of models could explicitly account for dependencies induced by grouping by associating random effects to data of the same grouping level. The assumption of equality of variances is unnecessary because they can be modeled from data. Furthermore, mixed-effects models are robust against missing values (*ibid.*). Zuur et al. (2009) give a good introduction to application of mixed-effects models in ecology.

The models were built using the package "nlme" (Pinheiro et al., 2008) in R (R Development Core Team, 2008). For details on model building strategy the reader is referred to Bogner et al. (2010). Using mixed-effects models, we analyzed the corrected total C and N contents, pH and exchangeable cations (Al, Fe, H, Ca and Mg). It was not possible to model the large variation of Ca, Mg and Fe concentrations adequately. Thus, these data were log-transformed to achieve approximate normality. We avoided backtransformation and calculated the ratio of concentrations in preferential flow paths and soil matrix instead. Provided that the residuals of the models are normally distributed and homoscedastic, the ratio of concentrations can be calculated directly by taking the exponent (Manning, 1998).

The model parameters were estimated by REML (residual maximum likelihood), so that R^2, the usual measure of goodness-of-fit for least-squares estimates, is not defined. To check the model quality, we calculated Pearson's correlation coefficient between the observed and the predicted values and R^2_β, the amount of variance explained by fixed effects (Edwards et al., 2008). Motivated by the lack of measures equivalent to R^2, Edwards et al. (2008) proposed to compare the "full" mixed-effects model that includes all parameters with an "empty" one which includes only the intercept. They defined R^2_β, the amount of variance explained by fixed effects:

$$R^2_\beta = \frac{(q-1)\nu^{-1}F(\hat{\boldsymbol{\beta}}, \hat{\boldsymbol{\Psi}})}{1 + (q-1)\nu^{-1}F(\hat{\boldsymbol{\beta}}, \hat{\boldsymbol{\Psi}})}$$

where q is the number of estimated parameters of the "full" model, ν are the residual degrees of freedom and $F(\hat{\boldsymbol{\beta}}, \hat{\boldsymbol{\Psi}})$ is the F statistic for the Wald test of the null hypothesis that all model parameters but the intercept are zero, $\hat{\boldsymbol{\beta}}$ and $\hat{\boldsymbol{\Psi}}$ are the vector of estimated fixed effects and the estimated variance-covariance matrix of fixed effects, respectively. This approach allows to use only one model fit, so that random effects and error structure are identical between the "full" and the "null" models (*ibid.*).

3. Results

3.1. Flow regime

In our study, we defined preferential flow paths as dye stained areas. In a previous work, Bogner et al. (2010) identified predominant flow mechanisms based on stained patterns and statistical analysis. According to their results, roots constituted main preferential flow paths and induced macropore flow, especially in the topsoil. In addition, these authors stated that in the subsoil, root density decreased and inhomogeneous infiltration from preferential flow paths into the soil matrix caused unstable flow. Due to the large sand content (i.e. high permeability) they found strong interactions between preferential flow paths and soil matrix resulting in large stained objects.

The amount of stained area per depth (dye coverage) varied between the three plots (Figure 2). In summary, the mean dye coverages equalled 8–25% in the AE, 14–30% in the Bsh, 31–41% in the Bs, 31–76% in the Bw and 9–14% in the Bw/C horizons. Finally, the iodide patterns did not indicate any serious retardation of Brilliant Blue compared to infiltrating water (Bogner et al., 2010).

3.2. Principal component analysis

We retained the first four principal axis based on the broken stick model (Frontier, 1976). It states that if the total variance in a multivariate data set was distributed at random across principal components, then the proportion of explained variance b_k associated with the eigenvalue of the kth component would be:

$$b_k = \frac{1}{p} \sum_{i=k}^{p} \frac{1}{i}$$

where p is the number of principal components. If the eigenvalue of the kth principal component is larger than b_k, then it is non-trivial and should be retained. The percentage of variance explained by the first four principal components was 40.8%, 25.4%, 14.7% and 11.4% respectively. The first principal axis has positive scores for the topsoil (AE, Bsh and Bs) and negative ones for the subsoil (Bw/C). Especially matrix samples from the subsoil form a distinct cluster in the left lower corner of the biplot (Figure 3a).

The second principal component separates samples from preferential flow paths from matrix samples. Indeed, K and Na were applied with the tracer and show high loadings on the second axis. Furthermore, Mn seems to be affected by the tracer because of its high correlation with the second principal component. We suppose that Mn was reduced by iodide also present in the tracer solution and became mobile. Therefore, we excluded K, Na and Mn from further analysis as they have been influenced by the tracer application.

The third principal component separates the three experimental plots (Figure 3b), the fourth component (not shown here) identifies extreme points. In summary, the depth gradient causes the highest variation in the data, followed by tracer influence and differences between plots.

3.3. Modeling results

3.3.1. Total C, total N and C:N ratio

The content of total C and total N decreased with depth (C: from about 42 g kg^{-1} in AE to about 15 g kg^{-1} in Bw/C, N: from about 1.6 g kg^{-1} to 1.1 g kg^{-1} in Bw/C (median values over all three plots)) and had its maximum in the Bsh (C: 47 g kg^{-1} and N: 2.1 g kg^{-1} (median values over all three plots)). Similarly, the C:N ratio also decreased with depth and ranged between 27 in AE and 16 in Bw/C (median values over all three plots) (Figure 4). We observed variation between horizons of different plots suggesting a random effect for horizon within plot. Consequently, the total C and N contents and the C:N ratio were modeled as:

$$y_{ijk} = \beta_j + \beta_s \cdot \text{silt} + \beta_{PF} + b_{ij} + \varepsilon_{ijk},$$
$$i = 1, 2, 3, \quad j = 1, \ldots, 4, \quad k = 1, \ldots, n_{ij},$$
$$b_{ij} \sim N(0, \sigma_1^2), \quad \varepsilon_{ijk} \sim N(0, \sigma^2 \delta_i^2)$$

$$\tag{1}$$

7
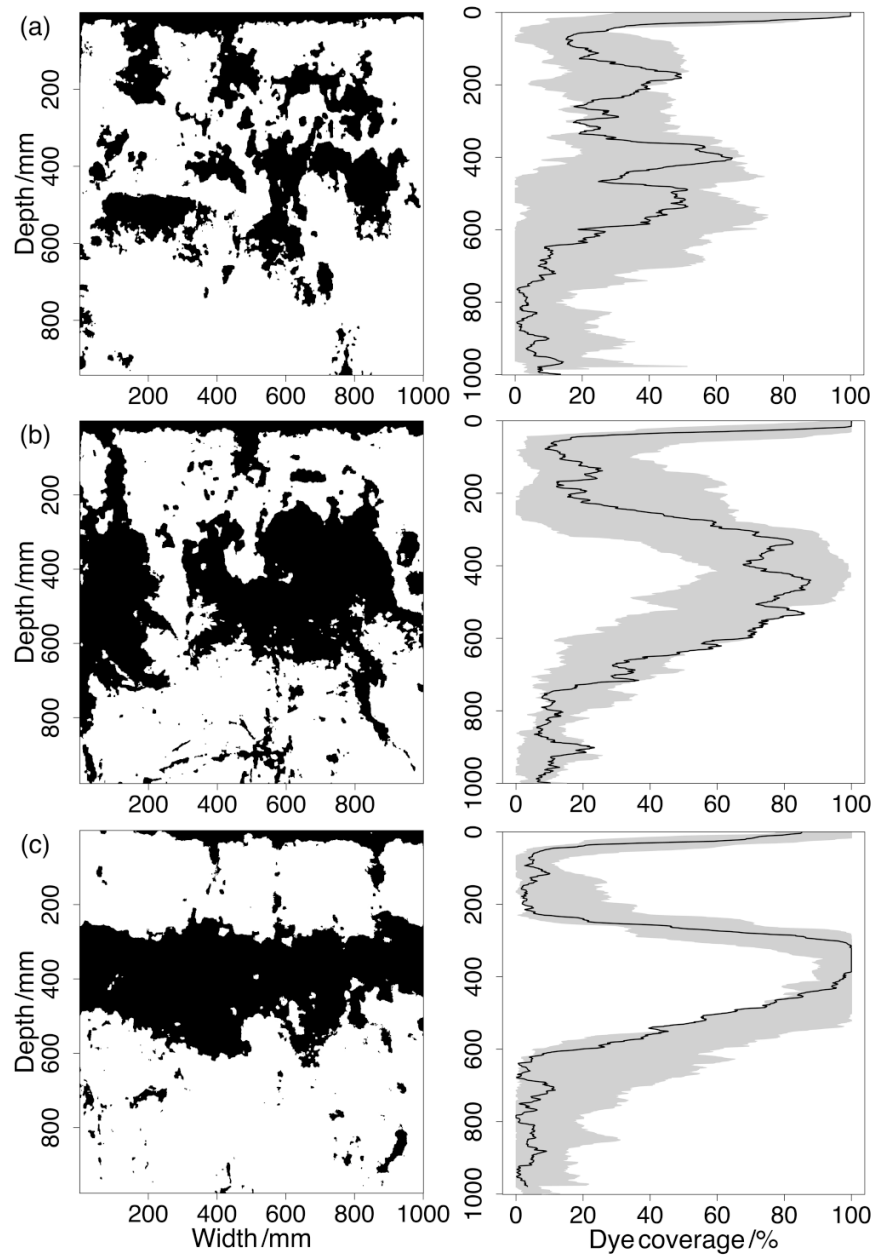
Figure 2: Typical infiltration patterns (left) and their dye coverages (solid lines on the right). The experimental plots 1 to 3 are indicated by (a) to (c). The gray area shows the variation of staining between minimum and maximum of all 11 profiles of a plot. Copyright © 2010 by John Wiley & Sons, Inc. Fig. 1 used with permission from Bogner et al. (2010).
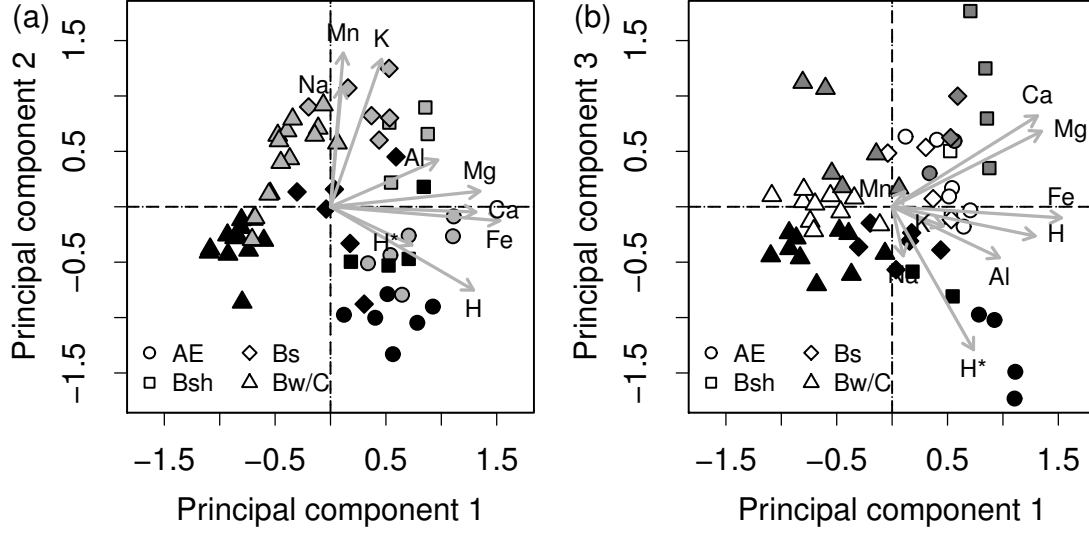
Figure 3: Biplots of the PCA with a scatter plot of component scores and eigenvector loadings as arrows. The variable H* denotes pH values transformed to hydronium concentrations per g soil. (a) matrix samples are shown in black, tracer samples in gray; (b) samples from plot 1 are plotted in black, from plot 2 in white and from plot 3 in gray.

where y_{ijk} is the content of C or N in g kg^{-1} or C:N ratio, β_j, β_s and β_{PF} are the fixed effects for horizon, content of silt and preferential flow, respectively, b_{ij} is the random effect for horizon within plot, ε_{ijk} the error term and n_{ij} the number of observation on plot i in horizon j. The error variance was not constant and was allowed to vary between plots, with δ_i^2 being the ratio of variances at different plots. For numerical stability, we mean-centered the silt content (i.e. subtracted the mean) and multiplied it by 0.1.

The fixed effects in model (1) explain 48%, 47% and 52% of variance of total C, total N and C:N ratio respectively. In addition, the correlation between fitted and observed values is 0.87, 0.82 and 0.73, respectively (Figure 5). The parameter β_{PF} that indicates the difference between preferential flow paths and soil matrix is significant. Hence, there are 5.0 g kg^{-1} more C ($P < 0.01$) and 0.24 g kg^{-1} more N ($P < 0.01$) in preferential flow paths than in soil matrix. Additionally, the C:N ratio is larger by 2 ($P < 0.01$) (Table 1).

3.3.2. pH

With decreasing depth pH values increased from 4.1 in AE to 4.5 in Bw/C (median values over all three plots). We observed the largest variability in the data between horizons and included a random effect for horizons within plots into the model:

$$y_{ijk} = \beta_j + \beta_{PF} + b_{ij} + \varepsilon_{ijk}, \tag{2}$$
$$i = 1, 2, 3, \quad j = 1, \ldots, 4, \quad k = 1, \ldots, n_{ij},$$
$$b_{ij} \sim N(0, \sigma_1^2), \quad \varepsilon_{ijk} \sim N(0, \sigma^2)$$

where y_{ijk} are pH values, β_j and β_{PF} are the fixed effects for horizon and preferential flow, respectively, b_{ij} is the horizon within plot random effect, ε_{ijk} the error term and n_{ij} the number of observation on plot i in horizon j.

9
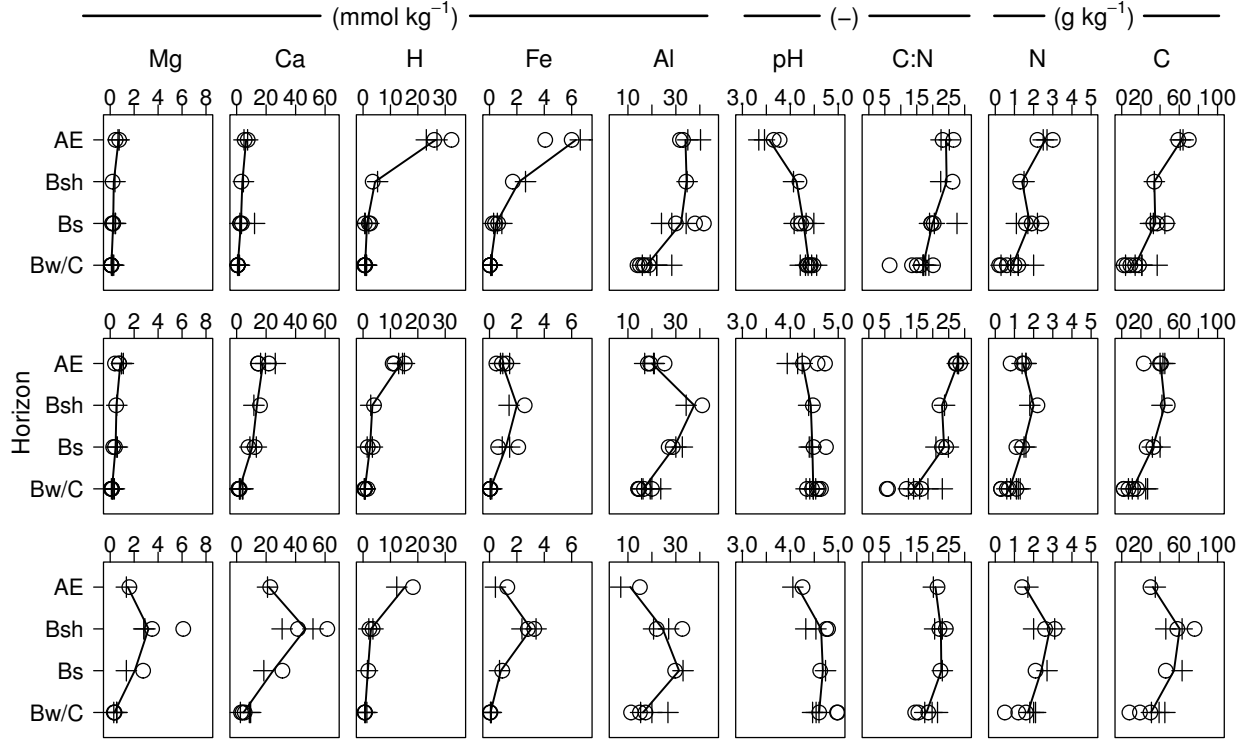
Figure 4: Variation of total C, total N, pH and exchangeable cations with depth. Panels from top to bottom show plots 1 to 3. Circles indicate samples from soil matrix, crosses are samples from preferential flow paths. The line connects median values of each horizon.

Table 1: Estimated fixed effects and their approximate 95% confidence intervals.

Parameter	C (g kg^{-1})	N (g kg^{-1})	C:N (–)	pH (–)
AE	52.14 (38.74, 65.53)	2.10 (1.49, 2.71)	25.83 (23.11, 28.55)	4.09 (3.77, 4.40)
Bsh	45.56 (32.52, 58.60)	2.02 (1.42, 2.62)	22.37 (19.84, 24.90)	4.47 (4.15, 4.79)
Bs	40.78 (27.75, 53.81)	1.86 (1.27, 2.45)	22.28 (19.91, 24.64)	4.56 (4.25, 4.87)
Bw/C	11.03 (−1.36, 23.42)	0.74 (0.17, 1.31)	13.68 (11.46, 15.89)	4.60 (4.29, 4.90)
β_{silt}	15.17 (9.05, 21.28)	0.67 (0.41, 0.93)	4.26 (1.79, 6.72)	–
β_{PF}	5.02 (1.46, 8.58)	0.24 (0.08, 0.39)	2.02 (0.67, 3.37)	−0.16 (−0.23, −0.08)
Al (mmol kg^{-1})	log(Fe (mmol kg^{-1}))	log(H (mmol kg^{-1}))	log(Ca (mmol kg^{-1}))	log(Mg (mmol kg^{-1}))
24.80 (17.25, 32.35)	0.24 (−0.50, 0.99)	2.85 (2.53, 3.17)	2.80 (1.67, 3.92)	0.01 (−1.32, 1.34)
32.37 (24.95, 39.78)	0.58 (−0.19, 1.35)	1.21 (0.88, 1.54)	2.59 (1.46, 3.71)	−0.31 (−1.63, 1.02)
31.80 (24.53, 39.07)	−0.55 (−1.29, 0.20)	0.49 (0.05, 0.94)	2.19 (1.07, 3.30)	−0.62 (−1.93, 0.70)
15.83 (8.79, 22.87)	−3.09 (−3.80, −2.38)	−0.33 (−0.66, −0.01)	0.45 (−0.66, 1.56)	−2.00 (−3.31, −0.70)
5.09 (1.20, 8.98)	–	–	0.45 (0.14, 0.77)	0.51 (0.19, 0.83)
1.21 (−0.97, 3.39)	0.51 (0.26, 0.76)	0.02 (−0.13, 0.18)	0.28 (0.08, 0.48)	0.41 (0.23, 0.59)

Table 2: Estimated random effects and within-group errors and their approximate 95% confidence intervals.

Modeled quantity	Plot	Horizon	Within-group error
C (g kg^{-1})	–	10.0 (5.4, 18.5)	6.1 (4.8, 7.8)
N (g kg^{-1})	–	0.5 (0.3, 0.8)	0.4 (0.3, 0.5)
C:N (–)	–	1.4 (0.5, 3.6)	3.3 (2.6, 4.2)
pH (–)	–	0.3 (0.1, 0.4)	0.1 (0.1, 0.2)
Al (mmol kg^{-1})	–	5.7 (3.2, 10.2)	4.1 (3.4, 5.1)
log(Fe mmol kg^{-1})	–	0.6 (0.3, 1.0)	0.5 (0.4, 0.6)
log(H mmol kg^{-1})	–	0.2 (0.1, 0.5)	0.2 (0.1, 0.5)
log(Ca mmol kg^{-1})	0.9 (0.3, 2.6)	–	0.4 (0.3, 0.5)
log(Mg mmol kg^{-1})	0.9 (0.3, 2.4)	0.3 (0.1, 0.7)	0.3 (0.3, 0.4)
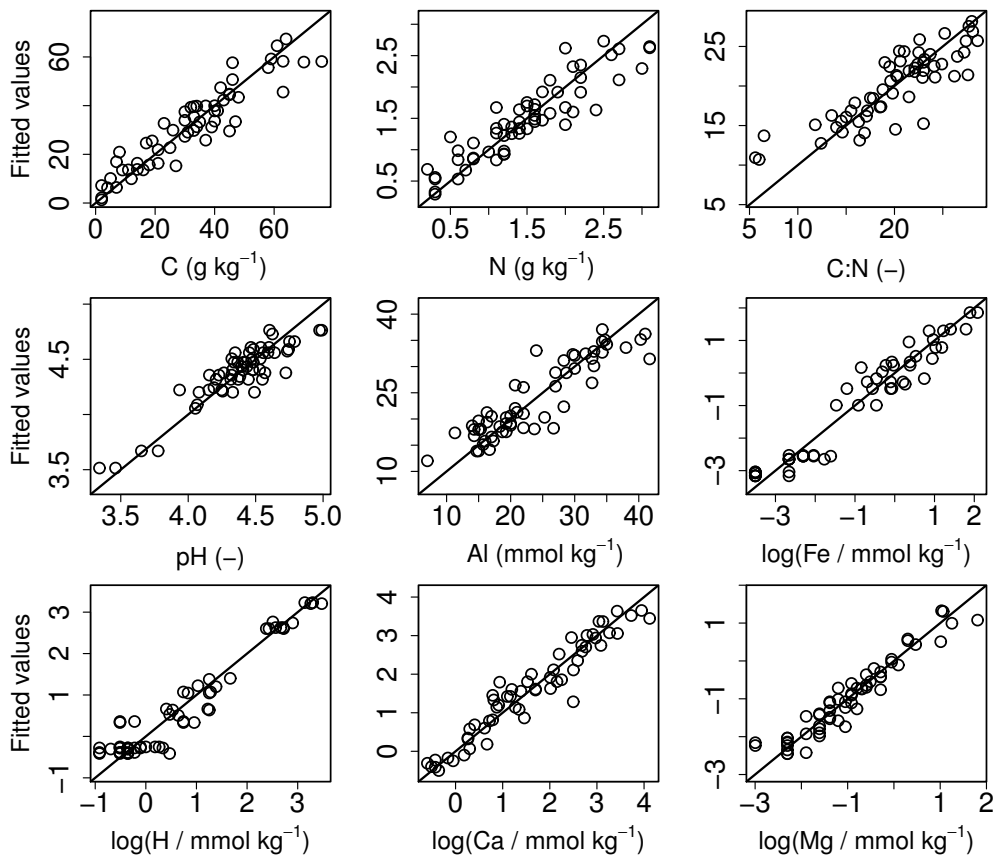
Figure 5: Results from mixed-effects modeling: fitted versus observed values. A straight line with slope 1 was added for better visibility.

The fixed effects in model (2) explain 31% of variance and the correlation between fitted and observed values equals 0.82 (Figure 5). The pH values are 0.16 units lower in preferential flow paths than in soil matrix ($P < 0.001$) (Table 1).

3.3.3. Al and Fe

The content of Al increased from 20.9 mmol kg^{-1} in AE to 33.5 mmol kg^{-1} in Bsh and decreased to 16.9 mmol kg^{-1} in Bw/C (median values over all three plots). In addition, we noticed a large variability between Al contents in the same horizon on different plots (Figure 4) and incorporated a horizon within plot random effect:

$$y_{ijk} = \beta_j + \beta_s \cdot \text{silt} + \beta_{PF} + b_{ij} + \varepsilon_{ijk}, \tag{3}$$
$$i = 1, 2, 3, \quad j = 1, 2, 3,$$
$$k = 1, \ldots, 4, \quad l = 1, \ldots, n_{ij},$$
$$b_{ij} \sim N(0, \sigma_1^2), \quad \varepsilon_{ijk} \sim N(0, \sigma^2)$$

where y_{ijk} is the content of Al in mmol kg^{-1} soil, β_j, β_s and β_{PF} are the same as in model (1), b_{ij} is the horizon within plot random effect, ε_{ijk} the error term and n_{ij} the number of observation on plot i in horizon j. For numerical stability, we mean-centered the silt content (i.e. subtracted the mean) and multiplied it by 0.1.

The fixed effects in model (3) explain 27% of the variance and the correlation between observed and fitted values equals 0.81 (Figure 5). There is no significant difference between preferential flow path and soil matrix ($P = 0.37$) (Table 1).

The concentration of Fe varied similarly to that of Al. Indeed, it increased from 1.27 mmol kg^{-1} in AE to 2.60 mmol kg^{-1} in Bsh and decreased to 0.07 mmol kg^{-1} in Bw/C (median values over all three plots) (Figure 4). Fe was modeled as:

$$\log(y_{ijk}) = \beta_j + \beta_{PF} + b_{ij} + \varepsilon_{ijk}, \tag{4}$$
$$i = 1, 2, 3, \quad j = 1, 2, 3, \quad k = 1, \ldots, n_{ij},$$
$$b_{ij} \sim N(0, \sigma_1^2), \quad \varepsilon_{ijk} \sim N(0, \sigma^2)$$

where y_{ijk} is the content of Fe in mmol kg^{-1} soil, β_j and β_{PF} are the same as in model (3), b_{ij} is the horizon within plot random effect, ε_{ijk} the error term and n_{ij} the number of observation on plot i in horizon j.

The fixed effects in model (4) explain 61% of the variance in the data and the correlation between fitted and transformed values equals 0.94 (Figure 5). We avoided the backtransformation of the model parameters to the original scale. Instead, we calculated the ratio of concentrations between preferential flow paths and soil matrix as $\exp(\beta_{PF})$. Hence, we obtain 67% more iron in the preferential flow paths than in soil matrix ($P < 0.001$).

3.3.4. H

We found a large amount of hydronium in AE (15.2 mmol kg^{-1}). It decreased to 0.7 mmol kg^{-1} in Bw/C and varied between the same horizons at different plots (Figure 4) suggesting a horizon within plot random effect:

$$\log(y_{ijk}) = \beta_j + \beta_{PF} + b_{ij} + \varepsilon_{ijk}, \tag{5}$$
$$i = 1, 2, 3, \quad j = 1, 2, 3, \quad k = 1, \ldots, n_{ij},$$
$$b_{ij} \sim N(0, \sigma_1^2), \quad \varepsilon_{ijk} \sim N(0, \sigma^2 \delta_j^2)$$

where y_{ijk} is the concentration of hydronium in mmol kg^{-1} and the other parameters are the same as in model (4). Despite the log-transformation the error variance was not constant and was allowed to differ between horizons, with δ_j^2 being the ratio of variances in different horizons.

The variance explained by fixed effects equals 79% and the correlation between the transformed observed and the fitted values is 0.95 (Figure 5). There is no significant difference in hydronium concentrations between the soil matrix and preferential flow paths ($P = 0.75$) (Table 1).

3.3.5. Ca and Mg

In summary, the concentrations of Ca decreased from 15.45 mmol kg^{-1} in AE to 1.68 mmol kg^{-1} in Bw/C with a maximum of 23.35 mmol kg^{-1} in Bsh (median values over all three plots). Figure 4 clearly shows a high variability between the tree plots which suggests a plot random effect:

$$\log(y_{ij}) = \beta_j + \beta_s \cdot \text{silt} + \beta_{PF} + b_i + \varepsilon_{ij}, \tag{6}$$
$$i = 1, 2, 3, \quad j = 1, \dots n_i,$$
$$b_i \sim N(0, \sigma_1^2), \quad \varepsilon_{ij} \sim N(0, \sigma^2)$$

where y_{ij} is the concentration of Ca in mmol kg^{-1} soil, β_j, β_s and β_{PF} are the fixed effects for horizon, content of silt and preferential flow, respectively, b_i is the plot random effect, ε_{ij} the error term and n_i the number of observations on plot i.

The explained variance equals 87% and the correlation between fitted and transformed values 0.92 (Figure 5). We calculated the ratio of concentrations and found 32% more Ca in preferential flow paths than in soil matrix ($P < 0.01$).

Similar to Ca, concentrations of Mg increased from 0.75 ,mmol kg^{-1} in AE to 1.67 mmol kg^{-1} in Bsh and decreased to 0.20 mmol kg^{-1} in Bw/C (median values over all three plots). The variability of the data suggests a plot and a horizon within plot random effects (Figure 4):

$$\log(y_{ijk}) = \beta_j + \beta_s \cdot \text{silt} + \beta_{PF} + b_i + b_{ij} + \varepsilon_{ijk}, \tag{7}$$
$$i = 1, 2, 3, \quad j = 1, \dots 4, \quad k = 1, \dots, n_{ij,}$$
$$b_i \sim N(0, \sigma_1^2), \quad b_{ij} \sim N(0, \sigma_2^2), \quad \varepsilon_{ijk} \sim N(0, \sigma^2)$$

where y_{ijk} is the concentration of Mg in mmol kg^{-1} soil, the fixed effects are the same as in model (6), b_i is the plot random effect, b_{ij} the horizon within plot random effect, ε_{ijk} the error term and n_{ij} the number of observation on plot i in horizon j.

The correlation between the fitted and the transformed values equals 0.92 (Figure 5) and the explained variance 57%. We found 51% more Mg in preferential flow paths than in soil matrix ($P < 0.001$).

4. Discussion

4.1. Goodness-of-fit

High correlation coefficients (> 0.8) between observed and predicted values indicate that the models fit the data accurately (Figure 5). The ratio of the confidence intervals to estimates

of the parameter β_{PF} varies between 0.3 (C) and 1.7 (Ca) (Table 1). Thus, despite a small data set, the differences between preferential flow paths and the soil matrix are estimated satisfactorily. The estimated random effects and their confidence intervals are larger than zero (Table 2) and show that our way of sampling induced dependencies in the data. The amount of variance explained by fixed effects ranges between 31% and 87%. The rest of variation is due to random effects and within-group errors.

Figure 4 indicates that differences between preferential flow and soil matrix might change between horizons suggesting an interaction effect. Especially for Al and pH, two models with the smallest amount of variance explained by fixed effects, one would expect such variations. For instance, there seems to be less Al in preferential flow paths in Bsh and more in Bw/C. However, the small data set did not support the fitting of any interaction effects because of a large natural variation in the field.

At our study site, silt was a good predictor for the content of total C and N, Al, Ca and Mg. The correlation of soil organic matter (SOM) with the content of silt was prior reported by Schmidt et al. (2000). They analyzed the accumulation of SOM in Aeh and Bh horizons of a podzol and found that the largest amount of C_{org} and N was contained in the silt fraction.

4.2. Variation of chemical parameters with depth and between plots

The three experimental plots are situated at the same study site only some 50 m apart. Nevertheless, they are quite different. The C and N profiles, for instance, varied remarkably between the plots (Figure 4). The largest values of total C an N were measured on plot 3 (C: 76 g kg^{-1}, N: 3.1 g kg^{-1}). On plot 2, the accumulation of SOM in Bsh was much less pronounced, and on plot 1 the C and N contents were larger in AE than in Bsh. Similarly, an accumulation of Al and Fe in Bsh and Bs was only visible on plots 2 and 3. In contrast, on plot 1 Fe concentration was largest in AE and Al concentrations remained constantly high from AE to Bs.

We attribute the differences in distributions of C, N, Al and Fe between plots to different degrees of podzolisation. Especially plot 1 distinguishes itself from the other two as it does not show any substantial accumulation of SOM and metal cations. Consequently, the random effects of plot and horizon within plot in our models are likely to reflect these different degrees of podzolisation.

As expected for a podzol, the C:N ratio was wide reflecting a low biological activity and a slow degradation of SOM (Figure 4). The largest and smallest values were measured on plot 2 (AE: 29, Bw/C: 6). While the values obtained in AE, Bsh and Bs agree well with Batjes (1996), the ratios measured in Bw/C are lower (16 vs. 25, mean values). The slow degradation of SOM can be ascribed to unfavorable chemical conditions. Beyer (1994), for instance, reported an accumulation of lignins in a podzol under spruce because a low supply in N and a low pH reduced the activity of lignolytic microorganisms.

Additionally, the C:N ratio at our study site decreased with depth indicating an older age of the SOM and a higher degree of decomposition in Bw/C. The C:N ratio as an indicator for the age of SOM was previously used by Batjes (1996). These findings agree well with mean radiocarbon signatures reported by Schulze et al. (2009) from the same study site. The authors reported modern C in litterfall and organic horizons and a highly variable range of $\Delta^{14}C$ signatures in AE. They also found a decrease in $\Delta^{14}C$ signatures and soil organic carbon from Bsh to Bw horizons.

4.3. Stability of preferential flow paths

The variable proportions of stained area show the importance of preferential flow at our site (Figure 2). Based on experimental evidence from other studies (Ritsema and Dekker, 2000; Hagedorn and Bundt, 2002) we suppose that many preferential flow paths remain stable down to the subsoil. Indeed, preferential flow along root channels dominates the flow system in the topsoil. In the subsoil, root density diminishes and inhomogeneous infiltration from preferential flow paths into the soil matrix takes place (Bogner et al., 2010). Consequently, as root channels remain stable for a long time (Hagedorn and Bundt, 2002), infiltration into the soil matrix in the subsoil is likely to occur at the same location.

Several studies showed that the irrigation rate (Gish et al., 2004) and in some soils the initial moisture (e.g. Flury et al., 1994; Hardie et al., 2011; Jarvis, 2007) influenced the extend of preferential flow. In our experiments, we did not vary these parameters, however, a previous work at the same study site indicated that preferential flow occurred at different moisture conditions and at different irrigation rates (64 and 32 mm h^{-1}) (Bogner et al., 2008). Moreover, the authors always observed the same flow regimes: preferential flow in the topsoil and heterogeneous matrix flow in the subsoil. Therefore, although we did not change the boundary and initial conditions, our experiments captured the main features of the flow processes.

4.4. Chemical properties of preferential flow paths

According to our modeling results, preferential flow paths have pH values lower by 0.16 units, 5.0 g kg^{-1} more C, 0.24 g kg^{-1} more N and a C:N ratio larger by 2. In addition, we found 67% more Fe, 32% more Ca and 51% more Mg. There are hints that aluminium content in preferential flow paths in Bw/C is higher, but as explained above the small data set does not support the fitting of interaction effects.

The larger C and N contents can be explained by root activity and transport of dissolved organic carbon (DOC) via preferential flow paths. Kuzyakov and Domanski (2000), stated that rhizodeposition of organic compounds, decomposition of dead roots and transport of DOC from organic to mineral horizons are major sources of organic C input to the mineral soil. Given the higher root density, roots contribute to the C input and facilitate the transport of DOC in preferential flow paths (Bogner et al., 2010). These findings agree well with results by Schulze et al. (2011) who analyzed the dynamics of the radiocarbon signature of DOC in soil solution beneath the Oa horizon and at 90 cm depth (horizon Bw/C) at the same study site. They found that DOC below organic horizons originated mainly from the overlaying Oa horizon; DOC signature in 90 cm depth, however, could not be explained by the Bs and Bw horizons as the only sources. These authors concluded that transport of DOC through preferential flow paths was likely.

A larger C:N ratio suggests that SOM in preferential flow paths is younger than in the soil matrix. This might be due to DOC transport from organic horizons because here C seems to be younger (Schulze et al., 2009). Additionally, an *in situ* exudation from living roots or decomposition of dead roots might contribute to young SOM. In their study Schulze et al. (2011) proposed rhizodeposition and microbial decomposition of dead roots as a source of young DOC.

Concerning lower pH values, we suppose that percolation of acid soil solution from organic horizons along root channels play an important role. Indeed, the lowest pH of this Podzol

was measured in the organic horizon (Hentschel et al., 2008). This accords well with our results which indicate an increase in pH values with depth (Figure 4).

A larger Fe concentration in preferential flow paths is probably linked to mobilization, downward transport and immobilization during podzolisation. Thereby, Al and Fe are mobilized in the AE horizon, eluviated downwards and sorbed mainly in the Bsh and Bs horizons. Along preferential flow paths these cations can be transported deeper to the horizon Bw/C. Moreover, lower pH values could favor the release of cations in soil solutions in preferential flow paths.

We attribute the elevated Ca and Mg concentration in preferential flow paths to transport from the soil surface after liming. This is in agreement with Jardine et al. (1989) who investigated the transport of organic and inorganic natural tracers (Mg, ammonium, bromide, nitrate and DOC) in a forest soil at saturated flow conditions. They observed skewed break through curves indicating preferential flow and concluded that a considerable quantity of Mg, ammonium, and DOC moved through soil via preferential flow paths. Therefore, increased concentrations of basic cations in preferential flow paths down to greater depth show that soil amelioration measures like liming could affect both the topsoil and subsoil horizons.

Larger Ca and Mg concentration and a lower pH in preferential flow paths seem to be a contradiction. However, several studies on long-term effects of liming of forest soils reported a fast dissolution of lime (e.g. Lorenz et al., 2001). Kreutzer (1995), for instance, observed that a dose of $4\,t\,ha^{-1}$ of dolomitic lime was dissolved completely within 6 years in a Norway spruce stand. Moreover, the increase of pH was restricted to the upper-most horizons (primarily the humus layer) and a reacidification by fresh litter took place (*ibid.*). After lime dissolution, a large amount of Ca and Mg were still retained in the soil (*ibid.*). At our study site, the lime application was accidental and diffuse and carbonate could not be detected at the time of our sampling (Hentschel et al., 2007). Nevertheless, large amounts of Ca and Mg were still found down to Bsh (*ibid.*) which accords well with findings by Kreutzer (1995) and Lorenz et al. (2001). Our results suggest that reacidification of preferential flow paths after liming is enhanced compared to the adjacent soil matrix probably by percolation of acid soil solution from organic soil horizons.

5. Conclusions

At our study site, preferential flow paths constitute a chemical environment with properties that are distinct from those encountered in the soil matrix with more C and N, a lower pH and more Fe. A lower pH might enhance the release of Fe (and possibly Al) and therefore increase the podzolisation process. However, the data basis in our study and the large natural variability did not allow to fit interaction effects. Consequently, we could not address the question whether differences between preferential flow and soil matrix vary with depth. Preferential flow does not only influence its immediate environment around paths, but also underlying horizons. Especially the impact on subsoil by preferential transport of basic cations has to be emphasized.

The measured chemical properties showed a large heterogeneity between plots and within horizons. Therefore, a higher spatial resolution of measurements could reveal more details. Particularly, differences between preferential flow paths along root channels and those in the soil matrix remained undiscovered. A promising technique to acquire data at a higher spatial

resolution is portable VIS-NIR diffuse reflectance spectroscopy. Its use for further tracer studies could address the question whether differences between preferential flow paths and soil matrix detected on bulk samples are the same on the scale of some cm^2.

Acknowledgements

References

Batjes, N., 1996. Total carbon and nitrogen in the soils of the world. European Journal of Soil Science 47, 151–163.

Beyer, L., 1994. Effect of cultivation on physico-chemical, humus-chemical and biotic properties and fertility of two forest soils. Agriculture, Ecosystems & Environment 48, 179–188.

Bogner, C., Gaul, D., Kolb, A., Schmiedinger, I., Huwe, B., 2010. Investigating flow mechanisms in a forest soil by mixed-effects modelling. European Journal of Soil Science 61, 1079–1090.

Bogner, C., Schmiedinger, I., Huwe, B., 2011. Rapid estimation of brilliant blue concentrations in soil by vis diffuse reflectance spectroscopy. Geoderma 164, 95–98.

Bogner, C., Wolf, B., Schlather, M., Huwe, B., 2008. Analysing flow patterns from dye tracer experiments in a forest soil using extreme value statistics. European Journal of Soil Science 59, 103–113.

Bundt, M., Jaggi, M., Blaser, P., Siegwolf, R., Hagedorn, F., 2001a. Carbon and nitrogen dynamics in preferential flow paths and matrix of a forest soil. Soil Science Society of America Journal 65, 1529–1538.

Bundt, M., Widmer, F., Pesaro, M., Zeyer, J., Blaser, P., 2001b. Preferential flow paths: biological 'hot spots' in soils. Soil Biology & Biochemistry 33, 729–738.

Buurman, P., Jongmans, A., 2005. Podzolisation and soil organic matter dynamics. Geoderma 125, 71–83.

Driessen, P., Deckers, J., Spaargaren, O., Nachtergaele, F., 2001. Lecture notes on the major soils of the world. http://www.fao.org/docrep/003/y1899e/y1899e00.htm. World Soil Resources Reports 49, FAO, Rome.

Edwards, L.J., Muller, K.E., Wolfinger, R.D., Qaqish, B.F., Schabenberger, O., 2008. An R^2 statistic for fixed effects in the linear mixed model. Statistics in Medicine 27, 6137–6157.

Flury, M., Flühler, H., 1994. Brilliant Blue FCF as a dye tracer for solute transport studies – a toxicological overview. Journal of Environmental Quality 23, 1108–1112.

Flury, M., Flühler, H., Jury, W.A., Leuenberger, J., 1994. Susceptibility of soils to preferential flow of water: a field study. Water Resources Research 30, 1945–1954.

Foken, T. (Ed.), 2003. Lufthygienisch-Bioklimatische Kennzeichnung des oberen Egertales. volume 100, 69+XLVIII of Bayreuther Institut für Terrestrische Ökosystemforschung (BITÖK). Bayreuther Forum Ökologie. In German.

Forrer, I.E., Papritz, A., Kasteel, R., Flühler, H., Luca, D., 2000. Quantifying dye tracers in soil profiles by image processing. European Journal of Soil Science 51, 313–322.

Frontier, S., 1976. Étude de la décroissance des valeurs propres dans une analyse en composantes principales: Comparaison avec le modèle du bâton brisé. Journal of Experimental Marine Biology and Ecology 25, 67–75. In French.

Gerstberger, P., Foken, T., Kalbitz, K., 2004. The Lehstenbach and Steinkreuz catchments in NE Bavaria, Germany, in: Matzner, E. (Ed.), Biogeochemistry of Forested Catchments in a Changing Environment. Springer Verlag, Berlin Heidelberg. volume 172 of *Ecological Studies*, pp. 15–44.

Ghodrati, M., Ernst, F.F., Jury, W.A., 1990. Automated spray system for application of solutes to small field plots. Soil Science Society of America Journal 54, 287–290.

Gish, T.J., Kung, K.J.S., Perry, D.C., Posner, J., Bubenzer, G., Helling, C.S., Kladivko, E.J., Steenhuis, T.S., 2004. Impact of preferential flow at varying irrigation rates by quantifying mass fluxes. Journal of Environmental Quality 33, 1033–1040.

Hagedorn, F., Bundt, M., 2002. The age of preferential flow paths. Geoderma 108, 119–132.

Hagedorn, F., Mohn, J., Schleppi, P., Flühler, H., 1999. The role of rapid flow paths for nitrogen transformation in a forest soil: A field study with micro suction cups. Soil Science Society of America Journal 63, 1915–1923.

Hardie, M.A., Cotching, W.E., Doyle, R.B., Holz, G., Lisson, S., Mattern, K., 2011. Effect of antecedent soil moisture on preferential flow in a texture-contrast soil. Journal of Hydrology 398, 191–201.

Hendrickx, J.M.H., Flury, M., 2001. Uniform and preferential flow mechanisms in the vadose zone, in: Council, N.R. (Ed.), Conceptual Models of Flow and Transport in the Fractured Vadose Zone. National Academy Press, Washington, DC, pp. 149–187.

Hentschel, K., Borken, W., Matzner, E., 2007. Leaching losses of inorganic N and DOC following repeated drying and wetting of a spruce forest soil. Plant and Soil 300, 21–34.

Hentschel, K., Borken, W., Matzner, E., 2008. Repeated freeze-thaw events affect leaching losses of nitrogen and dissolved organic matter in a forest soil. Journal of Plant Nutrition and Soil Science 171, 699–706.

IUSS Working Group WRB, 2007. World reference base for soil resources 2006, first update 2007. World Soil Resources Reports No. 103. http://www.fao.org/ag/agl/agll/wrb/doc/wrb2007_corr.pdf. [Accessed on 21-June-2010].

Jardine, P.M., Wilson, G.V., Luxmoore, R.J., McCarthy, J.F., 1989. Transport of inorganic and natural organic tracers through an isolated pedon in a forest watershed. Soil Science Society of America Journal 53, 317–323.

Jarvis, N.J., 2007. A review of non-equilibrium water flow and solute transport in soil macropores: principles, controlling factors and consequences for water quality. European Journal of Soil Science 58, 523–546.

Kasteel, R., Vogel, H.J., Roth, K., 2002. Effect of non-linear adsorption on the transport behaviour of Brilliant Blue in a field soil. European Journal of Soil Science 53, 231–240.

Ketelsen, H., Meyer-Windel, S., 1999. Adsorption of Brilliant Blue FCF by soils. Geoderma 90, 131–145.

Kreutzer, K., 1995. Effects of forest liming on soil processes. Plant and Soil 168-169, 447–470.

Kuzyakov, Y., Domanski, G., 2000. Carbon input by plants into the soil. Review. Journal of Plant Nutrition and Soil Science 163, 421–431.

Lorenz, K., Preston, C.M., Feger, K.H., 2001. Long-term effects of liming on microbial biomass and activity and soil organic matter quality (^{13}C CPMAS NMR) in organic horizons of Norway spruce forests in Southern Germany. Journal of Plant Nutrition and Soil Science 164, 555–560.

Lu, J., Wu, L., 2003. Visualizing bromide and iodide water tracer in soil profiles by spray methods. Journal of Environmental Quality 32, 363–367.

Lundström, U.S., van Breemen, N., Bain, D., 2000. The podzolization process. A review. Geoderma 94, 91–107.

Manning, W.G., 1998. The logged dependent variable, heteroscedasticity, and the retransformation problem. Journal of Health Economics 17, 283–295.

McKeague, J., DeConinck, F., Franzmeier, D., 1983. Spodosols, in: L.P. Wilding, N.S., Hall, G. (Eds.), Pedogenesis and Soil Taxonomy - II. The Soil Orders. Elsevier. volume 11, Part 2 of *Developments in Soil Science*, pp. 217 – 252.

Pinheiro, J., Bates, D., DebRoy, S., Sarkar, D., team, T.R.C., 2008. nlme: Linear and Nonlinear Mixed Effects Models. R package version 3.1-89.

Pinheiro, J.C., Bates, D.M., 2000. Mixed-Effects Models in S and S-Plus. Springer, New York.

R Development Core Team, 2008. R: A language and environment for statistical computing.

Ritsema, C.J., Dekker, L.W., 2000. Preferential flow in water repellent sandy soils: principles and modeling implications. Journal of Hydrology 231, 308–319. Sp. Iss. SI.

Sauer, D., Sponagel, H., Sommer, M., Giani, L., Jahn, R., Stahr, K., 2007. Podzol: Soil of the Year 2007. A review on its genesis, occurrence, and functions. Journal of Plant Nutrition and Soil Science 170, 581–597.

Schmidt, M.W.I., Knicker, H., Kögel-Knabner, I., 2000. Organic matter accumulating in Aeh and Bh horizons of a Podzol – chemical characterization in primary organo-mineral associations. Organic Geochemistry 31, 727–734.

Schulze, K., Borken, W., Matzner, E., 2011. Dynamics of dissolved organic ^{14}C in throughfall and soil solution of a Norway spruce forest. Biogeochemistry 106, 461–473.

Schulze, K., Borken, W., Muhr, J., Matzner, E., 2009. Stock, turnover time and accumulation of organic matter in bulk and density fractions of a podzol soil. European Journal of Soil Science 60, 567–577.

Vinther, F.P., Eiland, F., Lind, A.M., Elsgaard, L., 1999. Microbial biomass and numbers of denitrifiers related to macropore channels in agricultural and forest soils. Soil Biology and Biochemistry 31, 603–611.

Wuest, S.B., 2009. Comparison of preferential flow paths to bulk soil in a weakly aggregated silt loam soil. Vadose Zone Journal 8, 623–627.

Zuur, A.F., Ieno, E.N., Walker, N.J., Saveliev, A.A., Smith, G.M., 2009. Mixed effects models and extensions in ecology with R. Springer, New York.